

Robust UAV Path Planning with Obstacle Avoidance for Emergency Rescue

Junteng Mao[†], Ziye Jia^{†*}, Hanzhi Gu[†], Chenyu Shi[†], Haomin Shi[†], Lijun He^{*} and Qihui Wu[†]

[†]The Key Laboratory of Dynamic Cognitive System of Electromagnetic Spectrum Space, Ministry of Industry and Information Technology, Nanjing University of Aeronautics and Astronautics, Nanjing, Jiangsu, 211106, China

^{*}National Mobile Communications Research Laboratory, Southeast University, Nanjing, Jiangsu, 211111, China

^{*}The School of Information and Control Engineering, China University of Mining and Technology, Xuzhou 221116, China

{twistfate, jiaziye, hanzhi.gu, chenyu_Shi, shihaomin, wuqihui}@nuaa.edu.cn, lijunhe.xd@gmail.com

Abstract—The unmanned aerial vehicles (UAVs) are efficient tools for diverse tasks such as electronic reconnaissance, agricultural operations and disaster relief. In the complex three-dimensional (3D) environments, the path planning with obstacle avoidance for UAVs is a significant issue for security assurance. In this paper, we construct a comprehensive 3D scenario with obstacles and no-fly zones for dynamic UAV trajectory. Moreover, a novel artificial potential field algorithm coupled with simulated annealing (APF-SA) is proposed to tackle the robust path planning problem. APF-SA modifies the attractive and repulsive potential functions and leverages simulated annealing to escape local minimum and converge to globally optimal solutions. Simulation results demonstrate that the effectiveness of APF-SA, enabling efficient autonomous path planning for UAVs with obstacle avoidance.

Index Terms—UAV path planning, obstacle avoidance, enhanced artificial potential field method.

I. INTRODUCTION

IN recent years, unmanned aerial vehicles (UAVs) play increasingly important roles in applications of military mission, natural exploration, disaster relief, etc [1]. However, when the UAV flies autonomously in complex and changeable environments, how to effectively avoid obstacles and ensure flight safety becomes an urgent problem. Besides, in the process of searching unknown and complex environments, the finite energy capacity of UAVs imposes constraints on their service capabilities. To optimize mission execution, the autonomous path planning mechanisms are essential. Meanwhile, in order to accomplish multifarious monitoring, mapping, rescuing and searching tasks efficiently and safely, it is necessary for the UAV to have comprehensive obstacle avoidance abilities [2] [3]. Therefore, it is significant to study the autonomous path planning algorithm for UAVs with obstacle avoidance abilities.

This work was supported in part by National Natural Science Foundation of China under Grant 62301251 and 62201463, in part by the Natural Science Foundation on Frontier Leading Technology Basic Research Project of Jiangsu under Grant BK20222001, in part by the open research fund of National Mobile Communications Research Laboratory, Southeast University (No. 2024D04), in part by the Aeronautical Science Foundation of China 2023Z071052007, and in part by the Young Elite Scientists Sponsorship Program by CAST 2023QNRC001. (Corresponding author: Ziye Jia.)

Most existed researches on autonomous path planning and obstacle avoidance for UAVs are based on known environments. Traditional methods are classified as classic and heuristic approaches such as vector field histogram method and various geometry search algorithms (e.g. rapidly-exploring random tree star algorithm [4], Dijkstra's algorithm, Floyd's algorithm, A* algorithm, ant colony algorithm (ACO) [5], etc.). For example, authors in [6] proposed an improved ACO algorithm using a three-dimensional (3D) grid and a new weight-climbing parameter, which solved the problems of premature convergence and low efficiency of the traditional ACO algorithm. In [7], the authors used an improved A* algorithm to shorten the search cost and reduce the amount of search and inflection points successfully, making the path smoother and safer. Nevertheless, most algorithms suffer from overlong runtimes, excessive iterations, and low real-time processing capability. Therefore, it is essential to design a better algorithm to solve the obstacle avoidance and path planning problems for these complex environments.

The traditional artificial potential field (APF) method is widely used in UAV trajectory planning due to its advantages of simple calculations, outstanding real-time control, smooth path, laconic implementation, and convenient debugging [8]. However, UAVs are apt to be trapped into a local minimum and oscillations problem with traditional APF [9]. Besides, most researches on APF focused on two-dimensional environments, ignoring the shape and distribution of the obstacles in 3D terrain environments, especially when dealing with dynamic obstacles. In this regard, authors in [10] presented a UAV trajectory planning method utilizing a goal-biased APF in combination with the Rapidly exploring Random Tree star (RRT*) algorithm to improve the convergence speed and minimize the number of iterations. In [11], authors presented a rotating potential field methodology that enabled UAVs to avoid common local minima and oscillations effectively. However, these works fail to achieve smooth path planning and ignore the 3D dynamic environment.

Hence, in this work, we consider an unknown, complex

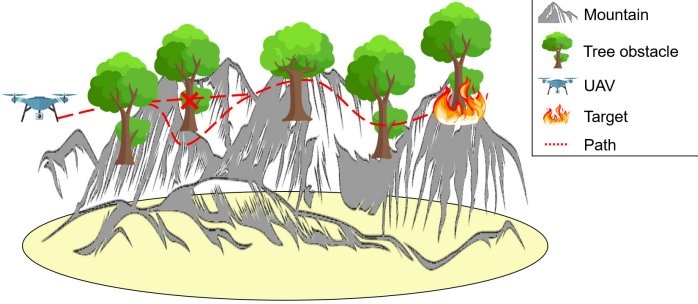


Fig. 1. Obstacle avoidance trajectory scenario for UAV in 3D environment.

forest firefighting environment with both dynamic and static obstacles. In particular, we model the ground obstacles, overhead obstacles, and dynamic obstacles that UAVs may encounter during its flight in the forest as cylinders, static spheres, and moving spheres, respectively. Then, we propose a novel artificial potential field algorithm based on simulated annealing (APF-SA), which significantly improves the conventional APF. Specifically, it amplifies the gravity function around the target point and introduces a repulsion correction factor to optimize the path towards the firefighting destination. Furthermore, the integration of simulated annealing (SA) techniques addresses the local minimum issue, enabling the algorithm to converge towards global optimal solutions. APF-SA aims to achieve fast firefighting safely and effectively through path planning autonomously with obstacle avoidance. Finally, we conduct simulations to verify the effectiveness of the proposed method.

The rest of the paper is organized as follows. The system model and problem formulation are presented in Section II. Then, the APF-SA algorithm is proposed in Section III. Simulations are conducted in Section IV, and finally conclusions are drawn in Section V.

II. SYSTEM MODEL AND PROBLEM FORMULATION

A. 3D Forest Scenario

As shown in Fig. 1, the UAV needs to perform the task of detecting fire in the mountains. We denote the 3D coordinate of target point, initiation point and UAV position as $X_g(x, y, z)$, $X_q(x, y, z)$ and $X_u(x, y, z)$, respectively. Considering the complex conditions in mountainous areas during the flight, the UAV may encounter a series of different obstacles $\mathbf{O} = (X_{o1}, X_{o2}, \dots, X_{oi}, \dots, X_{ol})$, including trees, no-fly zones, and other objects, where $X_{oi}(x, y, z)$ represents the barycenter of the i -th obstacle, and l denotes the total number of obstacles. In order to characterize the obstacles and perform 3D obstacle avoidance, different obstacles should be modeled independently. As for the obstacles of trees, we conceive them as cylinders with base radius r_1 and height h . The no-fly zone and other flying objects, are represented by spheres with radius r_2 and r_3 , respectively. Moreover, the positions of the flying objects' centers change over time, as shown in Fig. 2. In addition, the speed of the UAV during the flight changes with the variation of the resultant force. However, there exist

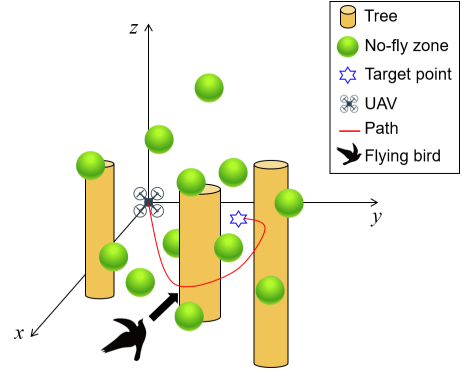


Fig. 2. Path planning model for UAV.

upper limitation to the power of UAV, so the speed range is $[v_{min}, v_{max}]$. In order to simplify the motion model of the UAV, the basic motion unit is set as a fixed step size Δs . If the driving direction of the UAV is $\delta(\gamma_x, \gamma_y, \gamma_z)$, the position update formula of the UAV is

$$\begin{cases} x' = x + \Delta s * \gamma_x, \\ y' = y + \Delta s * \gamma_y, \\ z' = z + \Delta s * \gamma_z, \end{cases} \quad (1)$$

wherein, γ_x represents the angle between the projection on the ground of the UAV's flight direction and the X-axis, while γ_y and γ_z indicate the angle with the Y-axis and the Z-axis, respectively.

Therefore, a series of track points can be obtained according to the preset step size and moving direction of the UAV. Moreover, we adopt the grid method to describe the 3D scenario, denoted as \mathcal{P} , which is a cuboid region of size $l_x \times l_y \times l_z$, consisting of several small cuboids with side length Δl . Hence, the number of small cubes is

$$N_x = \frac{l_x}{\Delta l}, N_y = \frac{l_y}{\Delta l}, \text{ and } N_z = \frac{l_z}{\Delta l}. \quad (2)$$

It is obvious that the hyperparameter Δl plays an important role in the whole grid construction, since the decrement of Δl results in an increment of N_x , N_y and N_z , and the whole 3D scenario can be more refined [12]. However, once the whole scenario reaches a certain scale, slightly reducing Δl can cause significant increment in the calculation cost, which is unacceptable. Therefore, it is significant to balance the size of the scenario with Δl to achieve detailed scene construction and acceptable calculation amplitude. Moreover, the position of the UAV should always be perceived for collision detection. In detail, $\rho(X_u, X_{oi})$ represents the distance between the UAV X_u and obstacle X_{oi} , i.e.,

$$\rho(X_u, X_{oi}) = \sqrt{(X_u - X_{oi})^2}. \quad (3)$$

Further, flag C_i represents collisions, i.e.,

$$C_i = \begin{cases} 1, & \rho(X_u, X_{oi}) \leq r_i, \\ 0, & \rho(X_u, X_{oi}) > r_i, \end{cases} \quad (4)$$

where r_i is the radius of obstacles. $C_i = 1$ indicates there is a collision between the UAV and an obstacle, and $C_i = 0$ otherwise.

B. Energy Cost Model

The finite maximum energy capacity W_{max} of the UAV during a mission imposes constraints on its payload and service capabilities [13]. Therefore, to ensure that the UAV can return smoothly during the execution of the task, we have:

$$\sum_{X_u=X_q}^{X_n} \Delta s \cdot \Delta w \leq W_{max}, \quad (5)$$

where Δw represents the energy consumed per unit length of the UAV trajectory and X_n is the coordinate position of the last point in the flight path of the UAV.

C. Problem Formulation

Since the purpose of the forest fire fighting problem is to reach the target as soon as possible by rationally planning the path of the UAV, the goal is to minimize the length of the route. Therefore, the optimization problem is formulated as:

$$\min_{X_u} \sum_{X_u=X_q}^{X_n} \Delta s \quad (6)$$

$$\text{s.t. } S \in \mathcal{P}, \quad (7)$$

$$\sum_{X_u=X_q}^{X_n} C_i = 0. \quad (8)$$

X_n , X_q and X_u represent the final location, start point, and the latest location of the UAV respectively. Therefore, we need to design a series of points that meet the requirements and obtain a short trajectory.

III. ALGORITHM DESIGN

A. Basic of APF

APF was first proposed by Khatib in 1986, and its basic principle is to simulate the motion of particles in a virtual potential field [14]. In this mechanism, the UAV is regarded as a particle, and then a gravitational field is set up around the target point from the UAV to the target. Generally, the gravity becomes stronger as the distance increases, attracting the UAV to move towards the target point. Meanwhile, a suitable repulsive force field is established around obstacles. The direction of repulsive force is from obstacles to the UAV, and its strength is usually inversely proportional to the distance of the UAV from the obstacle, allowing the UAV to avoid collisions with obstacles or no-fly zones. As shown in Fig. 3, the potential field function of APF can be expressed as the sum of the gravitational potential field and the repulsion potential field, i.e.,

$$U(X_u) = U_{att}(X_u) + U_{rep}(X_u), \quad (9)$$

where $U_{att}(X_u)$ is the gravitational potential field, and $U_{rep}(X_u)$ is the repulsive potential field. The corresponding gravitational or repulsive function can be obtained by finding the negative gradient of the potential field function. Since the

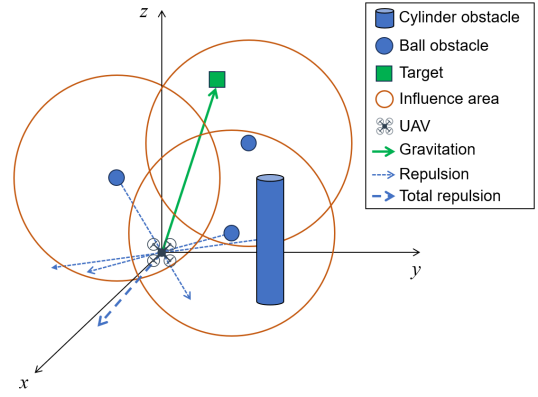


Fig. 3. APF principle.

motion of the UAV is constrained by the gravitational and repulsive forces, the resultant force can be expressed as:

$$F_s(X_u) = F_{att}(X_u) + F_{rep}(X_u), \quad (10)$$

where $F_{att}(X_u)$ denotes the gravitational force, directed by the UAV towards the target point, so that the UAV can approach the target. $F_{rep}(X_u)$ represents the repulsive force, and the direction is the reverse direction of the connection between the UAV and obstacles, enabling the UAV to avoid obstacles.

In order to further analyze the force on the UAV, the repulsive force and the attractive force can be calculated separately. The gravitational potential field is expressed as $U_{att}(X_u)$, whose size is determined by the relative distance between the UAV and the target point, and it always pulls the UAV to move towards the target point, i.e.,

$$U_{att}(X_u) = \frac{1}{2}\eta(X_u - X_g)^2, \quad (11)$$

in which η represents the attractive force gain coefficient. On this basis, the negative gradient of the gravitational potential field function can be obtained as:

$$F_{att}(X_u) = -\eta(X_u - X_g). \quad (12)$$

Similarly, the repulsive force potential field of obstacles to the UAV is $U_{rep}(X_u)$. The repulsive force increases when the UAV gets close to the obstacles. As such, the obstacle avoidance can be realized, and the repulsive field function is

$$U_{rep}(X_u) = \begin{cases} \frac{1}{2}\beta\left(\frac{1}{\rho(X_u, X_{oi})} - \frac{1}{\rho_0}\right)^2, & \rho(X_u, X_{oi}) < \rho_0, \\ 0, & \rho(X_u, X_{oi}) \geq \rho_0, \end{cases} \quad (13)$$

in which β is the repulsion gain constant, and ρ_0 indicates the maximum impact distance of a single obstacle.

B. Modified Potential Field Function

The main contributing factor for the unreachable target is that when approaching the target point, the gravitational force exerting on the UAV is too small, and the repulsive force received is too large, causing the UAV to yaw. Therefore, based

on the improved methods in [15], [16], APF-SA is decided to modify the gravitational function and repulsion function. Under the action of the original gravity function, although the UAV is close to the target point, the gravity also reduced. Therefore, when there are obstacles near the target point, the repulsive force received by the UAV may be greater than the gravitational force, resulting in the unreachable target point. Hence, it is necessary to increase the gravity appropriately near the target point without affecting other regions, and the corrected attractive function is

$$F_{att}(X_u) = -\eta[\rho(X_u, X_g) + e^{-(\rho(X_u, X_g) - \varepsilon \times \Delta s)}], \quad (14)$$

wherein, η is the attractive force gain, ε is the step size impact factor and $\rho(X_u, X_g)$ represents the relative distance between UAV X_u and goal point X_g .

As shown in Fig. 4, the attractive force intensifies as the UAV gets close to the target, enabling a successful arrival. When the UAV is located far from the target, its gravity remains largely consistent with the original gravity function. These observations validate the effectiveness of the revised gravity function. Meanwhile, the repulsion function is optimized and $\rho(X_u, X_g)$ is introduced, so that the repulsion force is not only related to the distance between the UAV and the obstacle, but also related to the distance between the UAV and target point. When the UAV gets close to the target point after the correction, the repulsive force of the obstacle gradually approaches zero. Hence, the target point becomes the lowest potential energy point, and the revised repulsion function is:

$$U_{rep}(X_u) = \begin{cases} \frac{1}{2}\beta\left(\frac{1}{\rho(X_u, X_{oi})} - \frac{1}{\rho_0}\right)^2 \rho(X_u, X_g)^\mu, & \rho(X_u, X_{oi}) < \rho_0, \\ 0, & \rho(X_u, X_{oi}) \geq \rho_0, \end{cases} \quad (15)$$

where $U_{rep}(X_u)$ is the revised repulsion field function. ρ_0 indicates the repulsion influence radius of the obstacle, and μ represents a positive real number, indicating the repulsive force near the target point is small enough, while the attractive force can still pull the UAV, thus solving the unreachable problem of the target point. As the negative gradient of the improved repulsion function, the repulsive force function is

$$F_{rep}(X_u) = \begin{cases} F_{repg1} + F_{repg2}, & \rho(X_u, X_{oi}) \leq \rho_0, \\ 0, & \rho(X_u, X_{oi}) > \rho_0, \end{cases} \quad (16)$$

wherein,

$$F_{repg1} = \beta\left(\frac{1}{\rho(X_u, X_{oi})} - \frac{1}{\rho_0}\right) \frac{\rho(X_u, X_g)^\mu}{\rho(X_u, X_{oi})^2} \frac{\partial \rho(X_u, X_{oi})}{\partial x}, \quad (17)$$

and

$$F_{repg2} = \frac{\mu}{2}\beta\left(\frac{1}{\rho(X_u, X_{oi})} - \frac{1}{\rho_0}\right)^2 \frac{\partial \rho(X_u, X_g)}{\partial x} \rho(X_u, X_g)^{\mu-1}. \quad (18)$$

The original repulsive force F_{repg1} points to the UAV from the obstacle. In order to avoid excessive repulsion, which causes the resultant force to deviate from the target point, a new

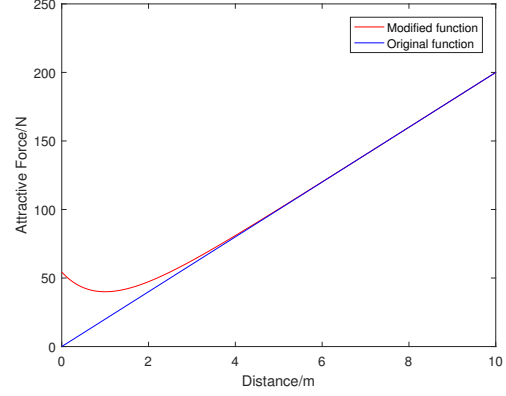


Fig. 4. Comparison of attractive force function original v.s. modified.

repulsion force F_{repg2} is added, which points toward the target point.

C. APF-SA Design

As mentioned in section III-A, the UAV is apt to fall into a local minimum area in the process of path planning. During the flight, there is a point where the gravitational force and the repulsive force are equal in magnitude but opposite in direction. This results in a zero resultant force on the UAV, causing it to lose directional information for its next movement. Consequently, the navigation algorithm fails, preventing the UAV from reaching its target. For this reason, the simulated annealing (SA) algorithm is adopted to randomly generate a new reachable trajectory point near the current position of the UAV, and make the UAV fly to this trajectory point. In this circumstance, the original force balance is broken, so that the UAV can break the local minimum dilemma and continue to move towards the target point.

SA is a generic probabilistic metaheuristics, initially introduced by Kirkpatrick *et al.* [17]. The algorithm is divided into an external cycle and an internal cycle, where the external cycle represents a drop in temperature, and the internal cycle is a different state at this temperature due to multiple random disturbances. The inner loop accepts the new state according to the Metropolis criterion [18], and the probability that the particle tends to equilibrium at temperature T is $p = e^{-\frac{\Delta E}{kT}}$, where E is the internal energy at temperature T , ΔE denotes the internal energy of change, and k represents the Boltzmann constant [19]. In detail, the Metropolis criterion is

$$p = \begin{cases} e^{-\frac{E(t_n) - E(t_0)}{T}}, & E(t_n) > E(t_0), \\ 1, & E(t_n) \leq E(t_0), \end{cases} \quad (19)$$

where t_n is the last time slot, and t_0 indicates the previous time slot. $E(t_0)$ is the internal energy at t_0 , $E(t_n)$ is the internal energy at t_n , and T stands for the current temperature. In the SA algorithm, the temperature T decreases as,

$$T(t) = \alpha T(t-1), \quad (20)$$

Algorithm 1 APF-SA.

Input: Starting point and target point.**Output:** Planned path and time consumption t .

- 1: *Initialization:* $t = 0$, start point X_q , target point X_g , UAV position X_u , target point produces F_{att} , and obstacles produce F_{rep} .
 - 2: **repeat**
 - 3: Calculate resultant force: $F_s = F_{att} + F_{rep}$.
 - 4: **if** $F_s = 0$ **then**
 - 5: Jump into SA (lines 7-8).
 - 6: **repeat**
 - 7: Add a random action point.
 - 8: Test whether the new point meets the requirements.
 - 9: **until** the new point is successful.
 - 10: Target the new point to escape local minima.
 - 11: **else**
 - 12: Calculate total force.
 - 13: Obtain new action point by step size.
 - 14: **end if**
 - 15: Move to the next point.
 - 16: Update X_u .
 - 17: **until** $X_u = X_g$.
-

wherein, α is a positive real number slightly less than 1, whose value is usually within (0.85, 1), and t is the number of iterations.

The specific process APF-SA is shown in Algorithm 1. The target point provides the attractive force for the UAV to fly close to the target, while the obstacles along the way provide a certain repulsive force to help the UAV successfully avoid obstacles (line 1). When the UAV is near the obstacle, it determines whether it enters the local minimum value (line 3). If it is not trapped, it flies through smoothly (lines 12-13). If it is trapped, it jumps into the simulated annealing process (lines 4-5). A new locus point X' is randomly generated at the current local minimum point X_u (line 7), and then it is judged whether the random point is located in the obstacle region. If not, the potential field at points X_u and X' is calculated respectively according to the potential field function (line 8). If the potential field of the random point is lower than that of the local minimum point, point X' is accepted as the next point (line 8). Otherwise, the point is accepted as the next point with probability p . This process keeps running until the end of the flight (line 17).

IV. SIMULATION RESULTS

Simulations are conducted in the following scenario: the UAV is treated as a particle and a $200\text{m} \times 200\text{m} \times 20\text{m}$ space is established in MATLAB R2021a. In order to verify the effectiveness of the proposed method, the local minimum problem, target unreachable problem and complex obstacle environment are tested.

To evaluate the performance of the proposed improved APF-SA, we compare the paths generated by the traditional APF algorithm with those generated by APF-SA in the same fixed

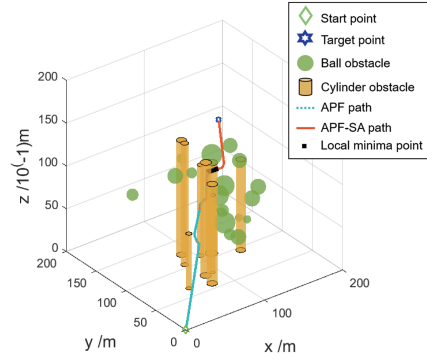


Fig. 5. Performance of local minimum with different methods.

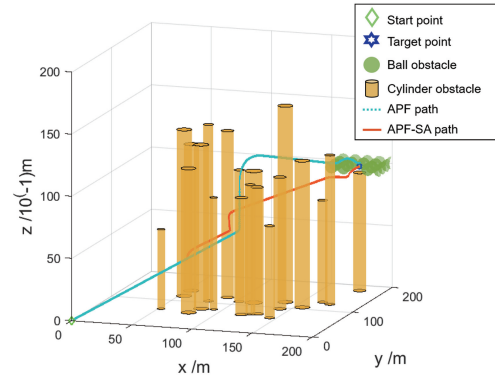


Fig. 6. Performance of unreachable target with different methods.

space. The flying environment in the forest is simulated by setting up spherical and cylindrical obstacles. As shown in Fig. 5, oscillation points are generated in the path of the traditional algorithm, and it is explained that the UAV is trapped in a local minimum. Meanwhile, APF-SA generates random track points in the path, and finally successfully breaks away from the local minimum dilemma and reaches the target point. Thus, Fig. 5 demonstrates the efficiency and effectiveness of APF-SA, when facing the local minimum problem.

Additionally, in Fig. 6, the path generated by APF-SA is more robust by modifying and optimizing the attractive and repulsive field functions. It is observed that in the complex obstacle avoidance environment, the traditional algorithm can not reach the target point, while APF-SA can achieve obstacle avoidance and reach the target well. Such target reachability demonstrates the robustness of APF-SA. Moreover, in Fig. 7, when dynamic obstacles are added to the scene, APF-SA also has excellent obstacle avoidance capacity, so it has good generalization performance and can handle static and dynamic obstacles well.

As shown in Fig. 8, we compare the traditional APF, RRT, RRT* and APF-SA algorithms. Simulation results show that the optimal path and average path of APF-SA are the shortest, and the worst path is slightly longer than that of RRT* when each algorithm runs 100 times. Therefore, APF-SA shows advantages in path length, time complexity, as well as resource efficiency.

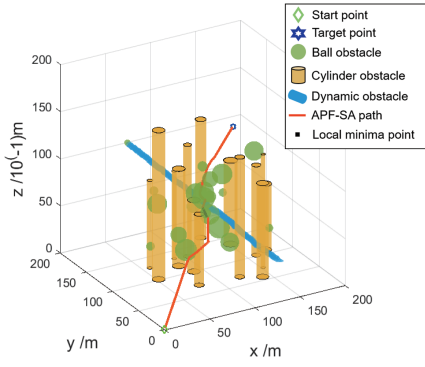


Fig. 7. Performance in complex space.

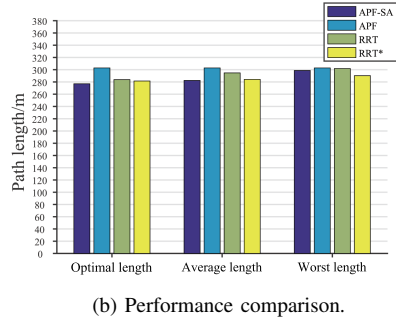
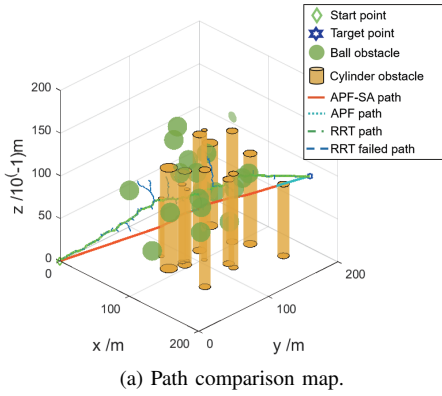


Fig. 8. Comparisons of multiple algorithms.

V. CONCLUSIONS

In this paper, we investigated the autonomous path planning of UAV based on obstacle avoidance function in 3D space for emergency rescue in forest scenarios. We employed cylindrical and spherical obstacles to respectively approximate forests and no-fly zones in the forest, and focused on navigating through complex obstacle environments. To handle the issues, we designed the APF-SA to obtain the optimized path efficiently. Simulation results showed that compared with the traditional APF, APF-SA obtained a better path and solved the problem of unreachable target to a great extent. Simulation results showed that APF-SA exhibited excellent obstacle avoidance performance under both static and dynamic obstacle environment.

REFERENCES

[1] Z. Lu, Z. Jia, Q. Wu, and Z. Han, "Joint trajectory planning and communication design for multiple UAVs in intelligent collaborative

air-ground communication systems," *IEEE Internet Things J.*, vol. 11, no. 19, pp. 31 053–31 067, Oct. 2024.

[2] C. DONG, Y. ZHANG, Z. JIA, Y. LIAO, L. ZHANG, and Q. WU, "Three-dimension collision-free trajectory planning of UAVs based on ADS-B information in low-altitude urban airspace," *Chin. J. Aeronaut.*, Apr. 2024.

[3] Z. Jia, J. You, C. Dong, Q. Wu, F. Zhou, D. Niyato, and Z. Han, "Cooperative cognitive dynamic system in UAV swarms: Reconfigurable mechanism and framework," *IEEE Veh. Technol. Mag.*, vol. 19, no. 3, pp. 90–101, Sep. 2024.

[4] M. Kim, J. Ahn, and J. Park, "TargetTree-RRT*: Continuous-Curvature Path Planning Algorithm for Autonomous Parking in Complex Environments," *IEEE Trans. Autom. Sci. Eng.*, vol. 21, no. 1, pp. 606–617, Jan. 2024.

[5] P. Wu, L. Zhong, J. Xiong, Y. Zeng, and M. Pei, "Two-level vehicle path planning model for multi-warehouse robots with conflict solution strategies and improved ACO," *J. Intell. Connected Veh.*, vol. 6, no. 2, pp. 102–112, Jun. 2023.

[6] Y. He, Q. Zeng, J. Liu, G. Xu, and X. Deng, "Path planning for indoor UAV based on Ant Colony Optimization," in *2013 25th Chinese Control and Decision Conference (CCDC)*, Guiyang, China, 2013, pp. 2919–2923.

[7] J. Li, X. Xiong, and Y. Yang, "A Method of UAV Navigation Planning Based on ROS and Improved A-star Algorithm," in *2023 CAA Symposium on Fault Detection, Supervision and Safety for Technical Processes (SAFEPROCESS)*, Yibin, China, 2023.

[8] S. Xie, J. Hu, P. Bhowmick, Z. Ding, and F. Arvin, "Distributed Motion Planning for Safe Autonomous Vehicle Overtaking via Artificial Potential Field," *IEEE Trans. Intell. Transp. Syst.*, vol. 23, no. 11, pp. 21 531–21 547, Nov. 2022.

[9] Q. Ma, M. Li, G. Huang, and S. Ullah, "Overtaking Path Planning for CAV Based on Improved Artificial Potential Field," *IEEE Trans. Veh. Technol.*, vol. 73, no. 2, pp. 1611–1622, Feb. 2024.

[10] X. Chen and J. Fan, "UAV trajectory planning based on APF-RRT* algorithm with goal-biased strategy," in *2022 34th Chinese Control and Decision Conference (CCDC)*, 2022, pp. 3253–3258.

[11] Z. Pan, C. Zhang, Y. Xia, H. Xiong, and X. Shao, "An Improved Artificial Potential Field Method for Path Planning and Formation Control of the Multi-UAV Systems," *IEEE Trans. Circuits Syst. II Express Briefs Transactions on Circuits and Systems II: Express Briefs*, vol. 69, no. 3, pp. 1129–1133, Mar. 2022.

[12] J. He, Z. Jia, C. Dong, J. Liu, Q. Wu, and J. Liu, "UAV Swarm Deployment and Trajectory for 3D Area Coverage via Reinforcement Learning," in *2023 International Conference on Wireless Communications and Signal Processing (WCSP)*, 2023, pp. 683–688.

[13] Z. Jia, M. Sheng, J. Li, D. Niyato, and Z. Han, "LEO-Satellite-Assisted UAV: Joint Trajectory and Data Collection for Internet of Remote Things in 6G Aerial Access Networks," *IEEE Internet Things J.*, vol. 8, no. 12, pp. 9814–9826, Jun. 2021.

[14] V. Dubey, B. Patel, and S. Barde, "Path Optimization and Obstacle Avoidance using Gradient Method with Potential Fields for Mobile Robot," in *2023 International Conference on Sustainable Computing and Smart Systems (ICSCSS)*, Coimbatore, India, 2023, pp. 1358–1364.

[15] Q. Fan, G. Cui, Z. Zhao, and J. Shen, "Obstacle Avoidance for Micro-robots in Simulated Vascular Environment Based on Combined Path Planning," *IEEE Rob. Autom. Lett.*, vol. 7, no. 4, pp. 9794–9801, Oct. 2022.

[16] A. Gottardi, S. Tortora, E. Tosello, and E. Menegatti, "Shared Control in Robot Teleoperation With Improved Potential Fields," *IEEE Trans. Hum.-Mach. Syst.*, vol. 52, no. 3, pp. 410–422, Jun. 2022.

[17] C. Li, F. You, T. Yao, J. Wang, W. Shi, J. Peng, and S. He, "Simulated Annealing Particle Swarm Optimization for High-Efficiency Power Amplifier Design," *IEEE Trans. Microwave Theory Tech.*, vol. 69, no. 5, pp. 2494–2505, May. 2021.

[18] S. Cao, R. Wang, and X. Du, "Performance Optimization of Variable Cycle Engine Based on Improved Simulated Annealing Algorithm," in *2022 8th International Conference on Control Science and Systems Engineering (ICCSSE)*, 2022, pp. 159–164.

[19] F. Okoli, J. Bert, S. Abdelaziz, N. BouSSION, and D. Visvikis, "Optimizing the Beam Selection for Noncoplanar VMAT by Using Simulated Annealing Approach," *IEEE Trans. Radiat. Plasma Med. Sci.*, vol. 6, no. 5, pp. 609–618, May. 2022.